Production of Z boson pairs at photon linear colliders

Duane A. Dicus
Center for Particle Physics, University of Texas at Austin, Austin, Texas 78712

Chung Kao
Department of Physics, B-159, Florida State University, Tallahassee, Florida 32306
(Received 8 September 1993)

The ZZ pair production rate in high energy $\gamma\gamma$ collisions is evaluated with photons from laser backscattering. We find that searching for the standard model Higgs boson with a mass up to, or slightly larger than, 400 GeV via the ZZ final state is possible via photon fusion with backscattered laser photons at a linear e^+e^- collider with energies in the range 600 GeV $< \sqrt{s_{e^+e^-}} <$ 1000 GeV.

PACS number(s): 13.85.Qk, 12.15.Ji, 14.70.Hp, 14.80.Bn

I. INTRODUCTION

In many cases, interesting physics processes can be studied with high precision at linear e^+e^- colliders where the background is usually low and the signal is much cleaner than that of hadron colliders. The Next Linear Collider (NLC) is a projected linear e^+e^- collider with a center of mass (c.m.) energy ($\sqrt{s_{e^+e^-}}$) of 500 GeV and a yearly integrated luminosity of about 10 fb^{-1}. In e^+e^- collisions, the Higgs boson of the standard model (SM) with a mass M_H up to 350 GeV [1,2] will be observable at the NLC. Improvements in the technology of laser backscattering have made it likely that the NLC could be run as a high energy photon collider [3–7]. Photon fusion can become a promising source to produce and study the Higgs bosons [8–12] of the SM and its extensions when the high energy $\gamma\gamma$ luminosity at linear e^+e^- colliders is greatly enhanced by laser backscattering. However, it was recently found [13, 14], that the transverse Z_TZ_T pair produced from photon fusion can become a serious irreducible background and make the Higgs boson search via the ZZ decay mode in $\gamma\gamma$ collisions impossible at the NLC and higher energy linear e^+e^- colliders if M_H is larger than about 350 GeV.

In this paper, the complete SM calculation of $\gamma\gamma \to ZZ$ is evaluated independently. A nonlinear gauge is used to greatly reduce the number of diagrams and simplify the Feynman rules. The total cross section and invariant mass distribution of ZZ pair at photon colliders is presented and the search for the SM Higgs boson is examined. Our cross sections of $\gamma\gamma \to ZZ$ for monochromatic photon collisions agree with that of Ref. [13] where a different nonlinear gauge was used, and Ref. [14] where a linear gauge was adopted and unpolarized initial e^+e^- and laser beams were considered. We have also checked the total cross section and invariant mass distribution for ZZ pair production with the polarizations of initial e^+e^- and laser beams as well as c.m. energies of e^+e^- considered in Ref. [13], and have found good agreement. In addition, we have considered other c.m. energies of e^+e^- and other polarizations of the electron positron and laser beams. Our conclusion as to a viability of a Higgs boson search with a realistic energy spectrum for backscattered photons is slightly more optimistic than that of Ref. [13] or [14].

II. NONLINEAR GAUGE FIXING AND LOOP INTEGRATION

In the SM, the lowest order $\gamma\gamma ZZ$ coupling comes from the one-loop diagrams of the leptons (l), the quarks (q), and the physical W boson ($W^\pm$) in the unitary gauge. The Higgs boson has a significant effect on the W loop and the top quark loop contributions. The Nambu-Goldstone boson ($G^\pm$) and the Faddeev-Popov ghosts ($\theta^\pm, \bar\theta^\pm$) play important roles in a general gauge and make W loop calculation unnecessarily complicated. It has been demonstrated for processes with photons that a carefully chosen nonlinear gauge [15–19] can remove the mixed vertices of photon-W-G($A^\mu W^\pm_\mu G^\mp$) and Higgs-photon-W-G ($HA^\mu W^\pm_\mu G^\mp$), reduce the number of loop diagrams and simplify the Feynman rules.

In this paper, a nonlinear R_ξ gauge is introduced to remove not only the mixed vertices γWG and γHWG but also the vertices ZWG and $ZHWG$. The gauge-fixing terms are chosen to be

$$\mathcal{L}_{\rm GF} = -\frac{1}{\xi_W} f^+ f^- - \frac{1}{2\xi_Z}(f^Z)^2 - \frac{1}{2\xi_A}(f^A)^2, \tag{1}$$

$$\begin{aligned} f^+ &= \partial^\mu W^+_\mu - i\xi_W M_W G^+ + ig' B^\mu W^+_\mu \\ &= \partial^\mu W^+_\mu - i\xi_W M_W G^+ \\ &\quad + ig\left(-\frac{\sin^2\theta_W}{\cos\theta_W} Z^\mu + \sin\theta_W A^\mu\right) W^+_\mu, \end{aligned} \tag{2}$$

$$f^Z = \partial^\mu Z_\mu - \xi_Z M_Z G^0, \tag{3}$$

$$f^A = \partial^\mu A_\mu, \tag{4}$$

where f^- is the Hermitian conjugate of f^+, M_W and M_Z are masses of the W and Z bosons, $g = e/\sin\theta_W$, and θ_W is the Weinberg angle. The ghost couplings that depend on the gauge fixing term (1) and all modified Feynman rules are given in an appendix. The gauge parameters are all taken to be unity, $\xi_W = \xi_Z = \xi_A = 1$, which corresponds to a nonlinear 't Hooft–Feynman gauge. In this new gauge, there are 3 pure classes of diagrams for the W boson (W loop), the Nambu-Goldstone boson (G loop), and the Faddeev-Popov ghosts (θ loop) with the same mass $M_W = M_G = M_\theta$. Further, the ghost loops contribute -2 times the Nambu-Goldstone boson loops except for those loops with a $ZZ\theta\theta$ coupling. In addition to the box (4-point) and the triangle (3-point) diagrams which appear in the fermion loops, there are also bubble (2-point) diagrams in the W, G, and θ loops: 24 box, 48 triangle, and 12 bubble diagrams without the Higgs boson; 8 triangle and 4 bubble diagrams with the Higgs boson; which add up to 96 diagrams in this gauge. In the linear R_ξ gauge [14], there are 188 diagrams: 108 box, 48 triangle, and 6 bubble diagrams without the Higgs boson; 20 triangle and 6 bubble diagrams with the Higgs boson. The fermion loops are obtained from an earlier calculation of $gg \to ZZ$ [20,21] with a modification of couplings. All loop integrations have been calculated with the computer program LOOP [22, 23], which evaluates one-loop integrals analytically and generates numerical data. The resulting numerical program is checked by replacing the polarization vector for one of the photons with its four-momentum. Gauge invariance requires that this yield a vanishing result which checks all integrals and algebra involved.

III. MONOCROMATIC $\gamma\gamma$ COLLISIONS

The amplitude of $\gamma\gamma \to ZZ$ can be written as

$$M_{\lambda_1\lambda_2\lambda_3\lambda_4} = \epsilon_1^\mu \epsilon_2^\nu \epsilon_3^\rho \epsilon_4^\sigma T_{\mu\nu\rho\sigma}(p_1, p_2, p_3, p_4), \qquad (5)$$

where $\lambda_{1,2}$ and $\lambda_{3,4}$ are the helicities of the photons and the Z's, the p's are the momenta, and the ϵ's are the polarization vectors.

The cross sections of $\gamma\gamma \to ZZ$ in different helicity states of ZZ are presented in Fig. 1 as a function of $\sqrt{s_{\gamma\gamma}}$ for both polarizations, $++$ and $+-$, of the photons. The parameters used are $\alpha = 1/128$, $\sin^2\theta_W = 0.230$, $M_Z = 91.17$ GeV, and $M_W = M_Z \cos\theta_W$. The Higgs boson mass (M_H) is taken to be 300, 400, 500, and 800 GeV. If not mentioned, the top quark mass (m_t) is considered to be 140 GeV. Also shown is the $++LL$ cross section without the Higgs boson, which is the same as taking $M_H = \infty$. As can be easily seen, the $Z_T Z_T$ cross section dominates and almost approaches a constant as $\sqrt{s_{\gamma\gamma}} > 1$ TeV, except for $M_H < 300$ GeV where the $++LL$ cross section is larger. Not shown are the individual contributions from the W loop and fermion loops. The W loop is usually at least about 10 times larger. Only in the $++LL$ state and for large m_t and high energy, can the top quark loop be comparable to the W loop; and only in the $++LT$ state at low energy, can the fermion loop dominate. For $M_H = \sqrt{s_{\gamma\gamma}} > 450$ GeV, the $++TT$ cross section is almost an order of magnitude larger than that of $++LL$, which makes the Higgs boson search in the ZZ mode via photon fusion impossible for $M_H > 450$ GeV, unless the transverse and longitudinal polarizations of the Z boson can be distinguished. All our numerical data agree with those in Ref. [13], except the cross section for $++LL$ cross section with $M_H = \infty$.

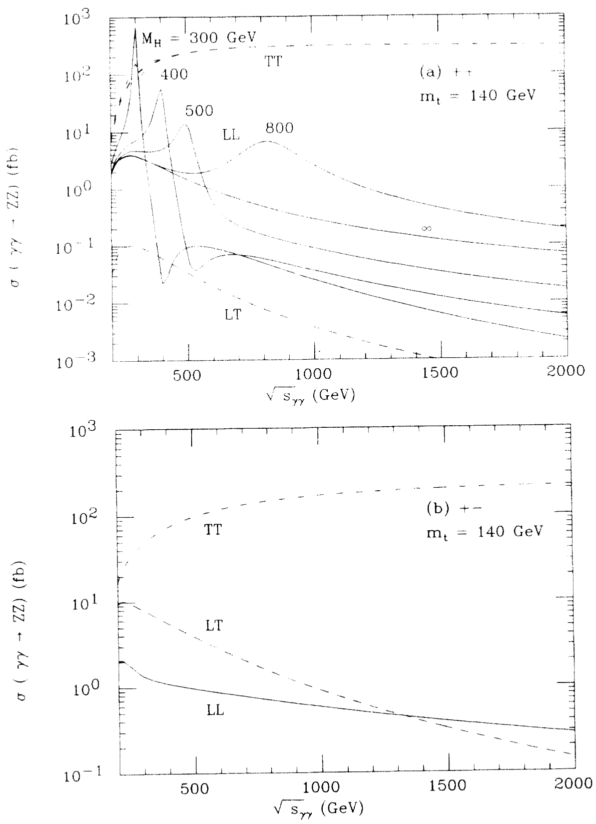

FIG. 1. The cross section of $\gamma\gamma \to ZZ$ as a function of $\sqrt{s_{\gamma\gamma}}$ for the LL (solid), TT (dash-dotted), and LT (dashed) helicity states of ZZ in (a) $++$ and (b) $+-$ helicity states of the photon with $m_t = 140$ GeV. The $++LL$ cross section is evaluated with $M_H = 300$, 400, 500, 800 GeV and ∞.

The m_t dependence and the interference between the W loop and fermion loop for the $++LL$ helicity states are shown in Fig. 2 for $m_t = 120, 160$, and 200 GeV. The W loop cross section is not sensitive to the top quark mass; it depends on m_t only in the Higgs boson width and therefore is evaluated with $m_t = 160$ GeV only. The

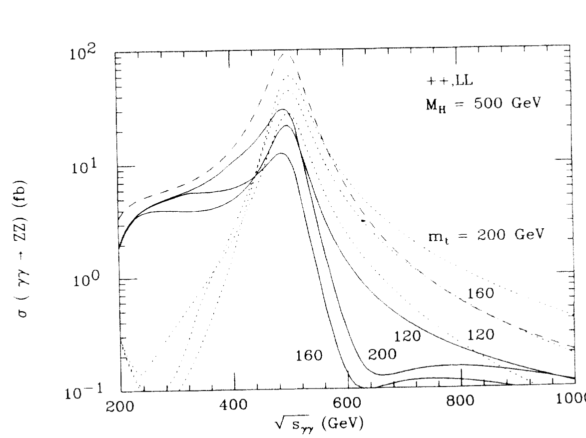

FIG. 2. The cross section of $\gamma\gamma \to ZZ$ as a function of $\sqrt{s_{\gamma\gamma}}$ in the $++LL$ state, for fermion loops alone (dotted), the W loop alone (dashed), and the sum of all loops (solid), with $m_t = 120$, 160, and 200 GeV and $M_H = 500$ GeV. The W loop cross section has been evaluated with $m_t = 160$ GeV.

TABLE I. The effect of m_t on the cross section of $\gamma\gamma ZZ$ in fb at $\sqrt{s_{\gamma\gamma}} = M_H = 300, 400, 500, 600, 700$, and 800 GeV, in the $++LL$ helicity state for $m_t = 120, 140, 160, 180$, and 200 GeV.

m_t (GeV)\\M_H (GeV)	300	400	500	600	700	800
120	360	55	22	14	11	9.4
140	660	57	13	8.1	7.1	6.6
160	790	87	11	4.2	4.0	4.2
180	810	160	16	2.6	1.8	2.4
200	830	210	29	3.3	0.69	1.1

total cross section at $\sqrt{s_{\gamma\gamma}} = M_H$ =300–800 GeV are also presented in Table I for m_t =120, 140, 160, 180, and 200 GeV where the precise value of m_t is used everywhere. Several interesting aspects can be learned from Fig. 2 and Table I. (1) The W loop and the fermion loop interfere destructively. (2) For M_H below 300 GeV, the total $++$ LL cross section grows with m_t, while for M_H above 700 GeV it decreases as m_t becomes larger. (3) For $M_H = 400, 500$, and 600 GeV there is a minimum which appears at about $m_t = 130, 160$, and 180 GeV, respectively. The $++LL$ cross section always depends on the m_t which appears in the Yukawa coupling of the top quark to the Higgs boson. Not shown is the TT cross section which becomes insensitive to m_t for $\sqrt{s_{\gamma\gamma}} > 500$ GeV.

The Higgs boson contributes only to the states with the same photon helicities and the same Z helicities. In order to improve the ratio of signal to background while saving most of the LL signal, we consider a cut on the c.m. scattering angle $|\cos(\theta^*)| = |z| < 0.8$ which reduces about 30% of the $++TT$, and more than 45% of the $+-TT$ background while saves about 80% of the $++LL$ signal. For the total cross section, the efficiency of this angular cut and one with $|z| < \cos(30°)$ are presented in Table II for $\sqrt{s_{\gamma\gamma}} = M_H = 300, 400$, and 500 GeV.

IV. BACKSCATTERED LASER $\gamma\gamma$ COLLISIONS

It has been shown that $\gamma\gamma ZZ$ can hardly be observed with the Weizsäcker-Williams photons [13], because the $\gamma\gamma$ luminosity falls rapidly as the $\gamma\gamma$ invariant mass increases. Fortunately, Compton laser backscattering can produce high energy photons with high luminosity. The total cross section of ZZ pair production at linear e^+e^- colliders with backscattered laser photons is evaluated from the differential cross section of the photon fusion subprocess $\gamma\gamma \to ZZ$ with the convolution of photon spectrum:

$$d\sigma_{\lambda_3\lambda_4} = \kappa \int_{4m_Z{}^2/s}^{y_m{}^2} d\tau \frac{dL_{\gamma\gamma}}{d\tau} \left(\frac{1+\langle\xi_1\xi_2\rangle}{2} d\hat{\sigma}_{++\lambda_3\lambda_4} + \frac{1-\langle\xi_1\xi_2\rangle}{2} d\hat{\sigma}_{+-\lambda_3\lambda_4} \right), \tag{6}$$

$$\frac{dL_{\gamma\gamma}}{d\tau} = \int_{\tau/y_m}^{y_m} \frac{dy}{y} f_{\gamma/e}(y,x) f_{\gamma/e}(\tau/y,x), \tag{7}$$

$$r = M_{ZZ}/\sqrt{s}, \tag{8}$$

$$\tau = \hat{s}/s = r^2, \tag{9}$$

$$y = E_\gamma/E_e, \tag{10}$$

$$y_m = \frac{x}{x+1}, \tag{11}$$

$$x = 4E_e\omega_0/m_e^2, \tag{12}$$

where $f_{\gamma/e}$ = photon energy distribution function, M_{ZZ} = the invariant mass of the ZZ pair, E_e = the initial electron energy, E_γ = backscattered photon energy, ω_0 = the laser photon energy, κ = number of high energy photons per one electron, and $\xi_{1,2}$ = the mean helicities of the photon beams. The maximal energy available in the c.m. frame of $\gamma\gamma$ is $E_{\max} = y_m\sqrt{s_{e^+e^-}}$. We have taken $\kappa = 1$, and $x = 4.8$ which gives $y_m = 0.83$. As noted in Ref. [6], if $x > 4.8$, number of high energy photons will be reduced by unwanted e^+e^- pair production. The $f_{\gamma/e}$ and ξ_i are taken from Eqs. (4), (12), and (17) of Ref. [4].

The energy spectrum of photons from Compton laser backscattering depends on the product $2\lambda_e\lambda_\gamma$ [4], where λ_e = the degree of polarization (mean helicity) of the initial electron (positron) and λ_γ = the degree of circular polarization or mean helicity of the laser beam. The number of high energy photons increases while the

TABLE II. The total cross section of $\gamma\gamma ZZ$ in fb at $\sqrt{s_{\gamma\gamma}} = M_H = 300, 400$, and 500 GeV, in each helicity state for $m_t = 140$ GeV after different cuts on the c.m. scattering angle $|\cos(\theta^*)| < z_0$: $z_0 = 1.0, \cos(30°)$ and 0.8.

z_0\\Helicities	$++LL$	$++TT$	$++LT$	$+-LL$	$+-TT$	$+-LT$
(a) $\sqrt{s_{\gamma\gamma}} = M_H = 300$ GeV						
1.0	660	160	0.099	1.4	47	8.0
cos (30°)	580	130	0.073	1.4	32	7.5
0.8	530	120	0.057	1.3	26	7.1
(b) $\sqrt{s_{\gamma\gamma}} = M_H = 400$ GeV						
1.0	57	180	0.061	1.1	74	5.5
cos (30°)	49	150	0.037	1.1	45	5.1
0.8	46	130	0.027	1.1	35	4.8
(c) $\sqrt{s_{\gamma\gamma}} = M_H = 500$ GeV						
1.0	13	240	0.034	0.96	98	3.9
cos (30°)	12	180	0.017	0.95	53	3.5
0.8	11	160	0.012	0.93	40	3.2

TABLE III. Total cross section of $\gamma\gamma \to ZZ$ in fb as a function of $\sqrt{s_{e^+e^-}}$ with backscattered laser photons for $|\cos(\theta^*)| < 0.8$, $m_t = 140$ GeV, $M_H = 300, 400$ GeV and ∞, and five combinations of polarizations of initial e^+e^- and laser beams with $\lambda_{e_1} = \lambda_{e_2} = \lambda_e$, and $\lambda_{\gamma_1} = \lambda_{\gamma_2} = \lambda_\gamma$.

M_H (GeV) \ $\sqrt{s_{e^+e^-}}$ (GeV)	240	300	400	500	600	700	1000
(a) $\lambda_e = 0.5$, $\lambda_\gamma = -1.0$							
300	0.55	8.9	62	48	58	67	76
400	0.47	7.7	30	54	59	66	75
∞	0.45	7.4	28	46	58	65	74
(b) $\lambda_e = 0.5$, $\lambda_\gamma = +1.0$							
300	2.8	1.5	18	44	61	78	104
400	2.7	1.3	10	27	47	63	96
∞	2.6	1.3	9.8	25	42	58	94
(c) $\lambda_e = 0$, $\lambda_\gamma = 0$							
300	0.39	4.5	26	37	48	57	72
400	0.38	4.3	16	30	42	52	70
∞	0.37	4.2	15	28	40	49	69
(d) $\lambda_e = 0.5$, $\lambda_\gamma = 0$							
300	0.19	4.1	38	49	62	72	89
400	0.17	3.6	18	39	54	67	87
∞	0.16	3.5	17	35	51	64	86
(e) $\lambda_e = 0$, $\lambda_\gamma = +1.0$							
300	0.29	4.8	25	35	47	55	77
400	0.27	4.4	16	30	40	51	71
∞	0.26	4.4	15	27	38	48	69

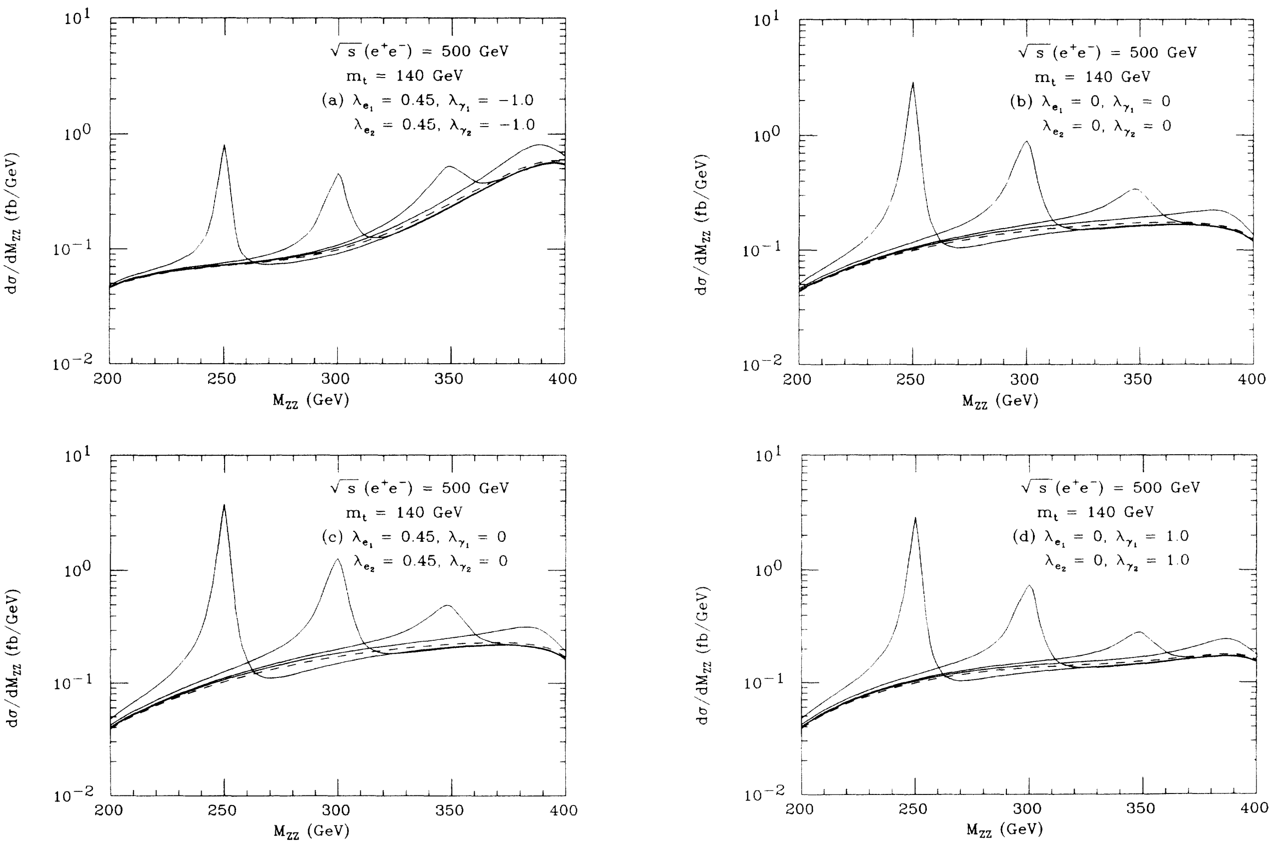

FIG. 3. Invariant mass distribution of $\gamma\gamma \to ZZ$ in high energy photon photon collisions from laser backscattered photons, for the NLC energy, $\sqrt{s_{e^+e^-}} = 500$ GeV, $m_t = 140$ GeV, and $M_H = 250$, 300, 350, and 390 GeV. The polarizations of the initial e^-e^+ and laser beams are taken to be (a) $\lambda_{e_1} = \lambda_{e_2} = 0.45$ and $\lambda_{\gamma_1} = \lambda_{\gamma_2} = -1.0$, (b) $\lambda_{e_1} = \lambda_{e_2} = 0$ and $\lambda_{\gamma_1} = \lambda_{\gamma_2} = 0$, (c) $\lambda_{e_1} = \lambda_{e_2} = 0.45$ and $\lambda_{\gamma_1} = \lambda_{\gamma_2} = 0$, and (d) $\lambda_{e_1} = \lambda_{e_2} = 0$ and $\lambda_{\gamma_1} = \lambda_{\gamma_2} = 1.0$.

number of soft photons decreases when $-2\lambda_e\lambda_\gamma$ becomes larger. We have studied the photon energy spectrum with $x = 4.8$ for three combinations of polarizations of the initial e^+e^- and laser beams: (a) $\lambda_e = 0.5$ and $\lambda_\gamma = -1.0$, polarized e^+e^- and laser beams with $2\lambda_e\lambda_\gamma = -1$; (b) $\lambda_e = 0.5$ and $\lambda_\gamma = 1.0$, polarized e^+e^- and laser beams with $2\lambda_e\lambda_\gamma = +1$; and (c) $\lambda_e = 0$ and $\lambda_\gamma = 0$, unpolarized e^+e^- and laser beams with $2\lambda_e\lambda_\gamma = 0$. Several interesting aspects have been found. (1) All of them produce about the same number of photons at an energy fraction $y_0 = E_\gamma/E_e = 0.7$. (2) Below y_0, the photon luminosity of case (b) is slightly larger than the others. However, it falls off rapidly for $y > y_0$. Case (a) rises sharply for $y > y_0$, but yields the smallest number of photons below y_0. (3) In case (c), $2\lambda_e\lambda_\gamma = 0$, the spectrum is almost flat below y_0, and the photon luminosity rises significantly as $y > y_0$. (4) In $\gamma\gamma$ collisions, the energy fractions y_1 and y_2 are related by $y_1y_2 = \tau$. With $\lambda_{e_1} = \lambda_{e_2} = \lambda_e$ and $\lambda_{\gamma_1} = \lambda_{\gamma_2} = \lambda_\gamma$, case (a) has the highest photon photon luminosity for $r = M_{ZZ}/\sqrt{s_{e^+e^-}} > 0.7$ while case (b) dominates for $r < 0.6$. Case (c) produces a larger number of photons in a broad range of energies.

Our main purpose is to enhance the Higgs boson signal as much as possible. The Stokes parameters $\langle\xi_1\xi_2\rangle$ in Eq. (6) play important roles in enhancing or reducing the Higgs boson signal. To study the effect of $\langle\xi_1\xi_2\rangle$ with $\lambda_{e_1} = \lambda_{e_2} = \lambda_e$ and $\lambda_{\gamma_1} = \lambda_{\gamma_2} = \lambda_\gamma$ in photon photon collisions, we have considered two more cases, (d) $\lambda_e = 0.5$ and $\lambda_\gamma = 0$, polarized e^+e^- and unpolarized laser beams; and (e) $\lambda_e = 0$ and $\lambda_\gamma = 1.0$, unpolarized e^+e^- and polarized laser beams; in addition to the three cases just considered for the photon energy spectrum. Since the Higgs boson appears only in the same helicity states of $\gamma\gamma ZZ$, we would like to enhance the cross section of $\hat\sigma_{++\lambda_3\lambda_4}$ while reducing $\hat\sigma_{+-\lambda_3\lambda_4}$. We have found that, in case (d), $\langle\xi_1\xi_2\rangle$ is always positive, and is enhanced as M_{ZZ} becomes larger. Case (b) usually has positive $\langle\xi_1\xi_2\rangle$ and it is the largest at low M_{ZZ}; however, it drops rapidly for $r > 0.7$. In case (a), $\langle\xi_1\xi_2\rangle$ is usually positive for $r < 0.30$ and $r > 0.63$, but usually negative in between. In case (c), $\langle\xi_1\xi_2\rangle = 0$. In case (e), $\langle\xi_1\xi_2\rangle$ is usually positive for $r < 0.54$ and $r > 0.76$, but becomes negative in between. The combination of polarizations $-\lambda_e$ and $-\lambda_\gamma$ has the same product $2\lambda_e\lambda_\gamma$ as that of λ_e and λ_γ, therefore produces the same energy spectrum but it yields $\langle\xi_1\xi_2\rangle$ with an opposite sign. As a combined effect from energy spectrum and the Stokes parameters, case (d) seems to be the best choice for the Higgs boson search over a broad range of M_H, case (a) is the best for $M_H > 0.7\sqrt{s_{e^+e^-}}$, and case (b) is the best for $M_H < 0.6\sqrt{s_{e^+e^-}}$.

The total cross section of $\gamma\gamma \to ZZ$ in high energy photon photon collisions with backscattered laser photons is presented as a function of $\sqrt{s_{e^+e^-}}$ in Table III, for $m_t = 140$ GeV and $m_H = 300, 400$ GeV and ∞ (the background) and the five combinations of polarizations for the initial e^+e^- and laser beams used for studying the Stokes parameters. From Table III we can find that (1) For M_H close to $E_{\max}$, $\lambda_{e_1} = \lambda_{e_2} = 0.5$ and $\lambda_{\gamma_1} = \lambda_{\gamma_2} = -1.0$ produces the largest cross section; (2) For M_H much smaller than $E_{\max}$, $\lambda_{e_1} = \lambda_{e_2} = 0.5$ and $\lambda_{\gamma_1} = \lambda_{\gamma_2} = 1.0$ produces the largest cross section; and (3) the unpolarized initial e^+e^- or laser beams, yield a clear Higgs boson signal for a broad range of energy.

To study the observability of the Higgs boson signal as a pronounced peak in the ZZ invariant mass distribution, we consider the total contribution without the Higgs boson as the background and show the Higgs boson signal with the background in Figs. 3 and 4. The invariant mass distribution of ZZ for $\gamma\gamma \to ZZ$ at

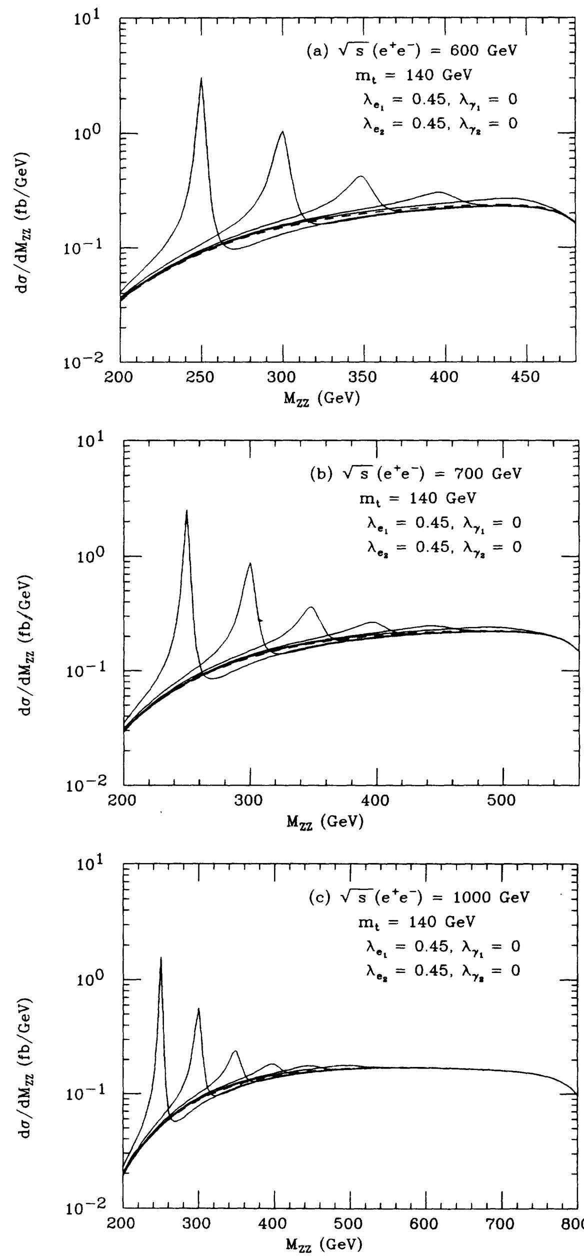

FIG. 4. Invariant mass distribution of $\gamma\gamma \to ZZ$ in high energy photon photon collisions from laser backscattered photons with polarizations of the initial e^-e^+ and laser beams being $\lambda_{e_1} = \lambda_{e_2} = 0.45$ and $\lambda_{\gamma_1} = \lambda_{\gamma_2} = 0$, for $m_t = 140$ GeV, $M_H = 250$, 300, 350, 400, 450, and 500 GeV, and (a) $\sqrt{s_{e^+e^-}} = 600$ GeV (without $M_H = 500$ GeV), (b) $\sqrt{s_{e^+e^-}} = 700$ GeV, and (c) $\sqrt{s_{e^+e^-}} = 1000$ GeV.

the NLC, $\sqrt{s_{e^+e^-}} = 500$ GeV, is shown in Fig. 3 for the three most promising polarizations of initial electron(positron) and laser beams: (a) $\lambda_{e_1} = \lambda_{e_2} = 0.45$ and $\lambda_{\gamma_1} = \lambda_{\gamma_2} = -1.0$, (b) $\lambda_{e_1} = \lambda_{e_2} = 0$ and $\lambda_{\gamma_1} = \lambda_{\gamma_2} = 0$, (c) $\lambda_{e_1} = \lambda_{e_2} = 0.45$ and $\lambda_{\gamma_1} = \lambda_{\gamma_2} = 0$, and also (d) $\lambda_{e_1} = \lambda_{e_2} = 0$ and $\lambda_{\gamma_1} = \lambda_{\gamma_2} = 1.0$, for completeness. The difference between λ_e's being 0.45 and 0.5 is about 5% for case (c) and less than 3% for case (a) in the invariant mass differential cross section. At the NLC, the Higgs boson signal appears as a pronounced peak in the ZZ invariant mass distribution, up to $M_H = 390$ GeV. We can find in Fig. 3 that the ratio of signal/background is enhanced for, $\lambda_{e_1} = \lambda_{e_2}$ close to $+0.5$ and $\lambda_{\gamma_1} = \lambda_{\gamma_2} = 0$ in a broad range.

Figure 4 shows that the Higgs boson signal for $M_H = 400$ GeV is visible in the invariant mass distribution of ZZ, at $\sqrt{s_{e^+e^-}} =$ (a) 600, (b) 700, and (c) 1000 GeV, in $\gamma\gamma$ collisions with photons from backscattered laser beams for $\lambda_{e_1} = \lambda_{e_2} = 0.45$ and $\lambda_{\gamma_1} = \lambda_{\gamma_2} = 0$. The cross sections at the Higgs boson pole for $\lambda_{e_1} = \lambda_{e_2} = 0$ and $\lambda_{\gamma_1} = \lambda_{\gamma_2} = 0$ are about 25% smaller. The combination of $\lambda_{e_1} = \lambda_{e_2} = 0$ and $\lambda_{\gamma_1} = \lambda_{\gamma_2} = \pm 1.0$ is slightly better than unpolarized e^+e^- and laser beams if $r < 0.5$ or $r > 0.8$. A more realistic study for the signal and background with the final states of $l^+l^-\nu\bar{\nu}$ and $l^+l^-q\bar{q}$ is under investigation.

V. CONCLUSIONS

In high energy $\gamma\gamma$ collisions, the TT cross section of $\gamma\gamma \to ZZ$ dominates if $M_H > 350$ GeV. With $2\lambda_e\lambda_\gamma = 0$, the photon spectrum is almost flat, and it is possible to search for the Higgs boson signal in a broad range below $\sqrt{s_{e^+e^-}}$. The best case to search for the Higgs boson signal is to have $\lambda_{e_1} = \lambda_{e_2}$ close to $+0.5$ and $\lambda_{\gamma_1} = \lambda_{\gamma_2} = 0$, because the photon energy spectrum is almost flat and the contribution from $\hat{\sigma}_{++LL}$ is enhanced by the Stokes parameters; however, even in the best case, using polarized electrons or laser photons yields only a small advantage over the totally unpolarized case. At the NLC, a Higgs boson signal is possible for M_H up to 390 GeV in the invariant mass distribution of ZZ. For larger c.m. energies, 600 GeV $< \sqrt{s_{e^+e^-}} <$ 1000 GeV, it is possible to find a Higgs boson with a mass slightly larger than 400

TABLE IV. The Feynman rules for relevant interactions involved in the W, G, and θ loops which appear in the reaction $\gamma\gamma \to ZZ$ as modified by the nonlinear gauge condition which is described in Sec. II. These can be compared to the unmodified rules given in Ref. [24]. (Note that not all of the rules below are modified.) All momenta (e.g., k, p, and q) and charges are incoming to the vertices. $g_{\mu\nu} \equiv \mathrm{diag}(+,-,-,-)$ is the metric tensor, s_W is $\sin\theta_W$, and c_W is $\cos\theta_W$.

3-point vertices	Feynman rules	4-point vertices	Feynman rules
$A_\mu(k)W^+_\nu(p)W^-_\rho(q)$	$-e[g_{\mu\nu}(k-p-q)_\rho$	$A_\mu A_\nu W^+_\rho W^-_\sigma$	$-2e^2 g_{\mu\nu}g_{\rho\sigma}$
	$+g_{\nu\rho}(p-q)_\mu$		
	$+g_{\rho\mu}(q-k+p)_\nu]$		
$A_\mu(k)G^+(p)G^-(q)$	$+e(p-q)_\mu$	$A_\mu A_\nu G^+G^-$	$+2e^2 g_{\mu\nu}$
$A_\mu(k)\theta^+(p)\bar{\theta}^+(q)$	$+e(p-q)_\mu$	$A_\mu A_\nu \theta^+\bar{\theta}^+$	$+2e^2 g_{\mu\nu}$
$A_\mu(k)\theta^-(p)\bar{\theta}^-(q)$	$-e(p-q)_\mu$	$A_\mu A_\nu \theta^-\bar{\theta}^-$	$+2e^2 g_{\mu\nu}$
$Z_\mu(k)W^+_\nu(p)W^-_\rho(q)$	$-gc_W\left[g_{\mu\nu}\left((k-p)_\rho + \frac{s_W^2}{c_W^2}q_\rho\right)\right.$	$Z_\mu Z_\nu W^+_\rho W^-_\sigma$	$-g^2c_W^2\left(2g_{\mu\nu}g_{\rho\sigma}\right.$
	$+g_{\nu\rho}(p-q)_\mu$		$-\frac{1-2s_W^2}{c_W^4}(g_{\mu\rho}g_{\nu\sigma}$
	$\left.+g_{\rho\mu}\left((q-k)_\nu - \frac{s_W^2}{c_W^2}p_\nu\right)\right]$		$\left.+g_{\mu\sigma}g_{\nu\rho})\right)$
$Z_\mu(k)G^+(p)G^-(q)$	$+\frac{1}{2}g\left(\frac{1-2s_W^2}{c_W}\right)(p-q)_\mu$	$Z_\mu Z_\nu G^+G^-$	$+\frac{1}{2}g^2\frac{(1-2s_W^2)^2}{c_W^2}g_{\mu\nu}$
$Z_\mu(k)\theta^+(p)\bar{\theta}^+(q)$	$-gc_W\left(\frac{s_W^2}{c_W^2}p_\mu + q_\mu\right)$	$Z_\mu Z_\nu \theta^+\bar{\theta}^+$	$-2e^2 g_{\mu\nu}$
$Z_\mu(k)\theta^-(p)\bar{\theta}^-(q)$	$+gc_W\left(\frac{s_W^2}{c_W^2}p_\mu + q_\mu\right)$	$Z_\mu Z_\nu \theta^-\bar{\theta}^-$	$-2e^2 g_{\mu\nu}$
$HZ_\mu Z_\nu$	$+\frac{g}{c_W}M_Z g_{\mu\nu}$	$Z_\mu A_\nu W^+_\rho W^-_\sigma$	$-egc_W\left(2g_{\mu\nu}g_{\rho\sigma}\right.$
$HW^+_\mu W^-_\nu$	$+gM_W g_{\mu\nu}$		$\left.-\frac{1}{c_W^2}(g_{\mu\rho}g_{\nu\sigma} + g_{\mu\sigma}g_{\nu\rho})\right)$
HG^+G^-	$-\frac{1}{2}g\frac{M_H^2}{M_W}$	$Z_\mu A_\nu G^+G^-$	$+eg\left(\frac{1-2s_W^2}{c_W}\right)g_{\mu\nu}$
$H\theta^\pm\bar{\theta}^\pm$	$-\frac{1}{2}gM_W$	$Z_\mu A_\nu \theta^\pm\bar{\theta}^\pm$	$+eg\left(\frac{1-2s_W^2}{c_W}\right)g_{\mu\nu}$

GeV. Thus there is not much advantage for this process in higher e^+e^- energies. Furthermore, there is not much advantage in the $\gamma\gamma$ mode; e^+e^- collisions at the NLC, by themselves, can search for the Higgs boson up to a mass of 350 GeV. The unique strength of high energy $\gamma\gamma$ collisions in the Higgs boson search is probably to measure the $H\gamma\gamma$ coupling with high precision beyond the intermediate Higgs boson mass range.

ACKNOWLEDGMENTS

The authors would like to thank David Bowser-Chao, Kingman Cheung, and George Jikia for discussions and Scott Willenbrock for suggestions and comments. This research was supported in part by DOE Contracts No. DE-FG03-93-ER40757 and No. DE-FG05-87-ER40319.

APPENDIX: RELEVANT FENYMAN RULES IN THE NONLINEAR GAUGE

In this appendix, relevant Feynman rules in the nonlinear gauge described in Sec. II are presented in our conventions. There are 3- and 4-point vertices among the gauge boson fields $W^{\pm}_{\mu}$, Z_μ, A_μ; the Nambu-Goldstone boson fields $G^{\pm}$, G^0; the Faddeev-Popov ghost fields $\theta^{\pm}$, $\bar{\theta}^{\pm}$, θ^Z, $\bar{\theta}^Z$, θ^A, $\bar{\theta}^A$; and the Higgs boson field H. The gauge parameters are all taken to be unity, $\xi_W = \xi_Z = \xi_A = 1$, which corresponds to a nonlinear 't Hooft–Feynman gauge. In this gauge, the W boson ($W^{\pm}$), the Nambu-Goldstone boson ($G^{\pm}$), and the Faddeev-Popov ghosts ($\theta^{\pm}$) have the same mass $M_W = M_G = M_\theta$. The Feynman rules for relevant interactions involved in the W, G, and θ loops which appear in the reaction $\gamma\gamma \to ZZ$ are shown in Table IV.

[1] V. Barger, K. Cheung, B. A. Kniehl, and R. J. N. Phillips, Phys. Rev. D **46**, 3725 (1992).

[2] J. F. Gunion, in Proceedings of the International Workshop on Physics and Experiments with Linear e^+e^- Colliders, Hawaii, 1993 (unpublished), and references therein.

[3] I. F. Ginzburg, G. L. Kotkin, V. G. Serbo, and V. I. Telnov, Nucl. Instrum. Methods **205**, 47 (1983).

[4] I. F. Ginzburg, G. L. Kotkin, S. L. Panfil, V. G. Serbo, and V. I. Telnov, Nucl. Instrum. Methods **219**, 5 (1984).

[5] T. L. Barklow, in *Research Directions for the Decade*, Proceedings of the Snowmass Summer Study, Snowmass, Colorado, 1990, edited by E. L. Berger (World Scientific, Singapore, 1991).

[6] V. I. Telnov, Nucl. Instrum. Methods **A294**, 72 (1990).

[7] D. L. Borden, D. A. Bauer, and D. O. Caldwell, SLAC Report No. SLAC-PUB-5715, 1992 (unpublished).

[8] J. F. Gunion and H. E. Haber, in *Research Directions for the Decade*, Proceedings of the Snowmass Summer Study, Snowmass, Colorado, 1990, edited by E. L. Berger (World Scientific, Singapore, 1991); J. F. Gunion and H. E. Haber, Phys. Rev. D **48**, 5109 (1992).

[9] H. E. Haber, in *Proceedings of the 1st International Workshop on Physics and Experiments with Linear e^+e^- Colliders*, Saariselkä, Finland, 1992, edited by R. Orava, P. Eerola, and M. Nordberg (World Scientific, Singapore, 1992).

[10] E. E. Boos and G. V. Jikia, Phys. Lett. B **275**, 164 (1992).

[11] J. F. Gunion, Report No. UCD-93-8, 1993 (unpublished).

[12] D. Bowser-Chao and K. Cheung, Phys. Rev. D **48**, 89 (1993).

[13] G. V. Jikia, Phys. Lett. B **298**, 224 (1993); Report No. IHEP 93-37, 1993 (unpublished).

[14] M. S. Berger, Phys. Rev. D **48**, 5121 (1993).

[15] K. Fujikawa, Phys. Rev. D **7**, 393 (1973).

[16] M. Bace and N. D. Hari Dass, Ann. Phys. (N.Y.) **94**, 349 (1975).

[17] M. Gavela, G. Girardi, C Malleville, and P. Sorba, Nucl. Phys. **B193**, 257 (1981).

[18] N. G. Deshpande and M. Nazerimonfared, Nucl. Phys. **B213**, 390 (1983).

[19] F. Boudjema, Phys. Lett. B **187**, 362 (1987).

[20] D. A. Dicus, C. Kao, and W. W. Repko, Phys. Rev. D **36**, 1570 (1987); D. A. Dicus, *ibid.* **38**, 394 (1988).

[21] E. W. N. Glover and J. J. van der Bij, Phys. Lett. B **219**, 488 (1989); Nucl. Phys. **B321**, 561 (1989).

[22] D. Dicus and C. Kao, LOOP, a FORTRAN program for doing loop integrations of 1, 2, 3, and 4 point functions with momenta in the numerator, 1991 (unpublished).

[23] G. 't Hooft and M. Veltman, Nucl. Phys. **B153**, 365 (1979); G. Passarino and M. Veltman, *ibid.* **B160**, 151 (1979).

[24] K.-I. Aoki *et al.*, Prog. Theor. Phys. Suppl. No. 73 (1982).